

# Dynamic Graph Representation for WSI Classification: A Knowledge-Aware Attention Mechanism for Enhanced Computational Pathology

T. Rajesh Kumar,  
Department of Computer Science and  
Engineering,  
Saveetha School of Engineering,  
Saveetha Institute of Medical and  
Technical Sciences,  
Chennai, Tamil Nadu, India-602105.  
t.rajesh61074@gmail.com

Dr. Mahaveerakannan R,  
Professor, Department of Computer  
Science and Engineering,  
Saveetha School of Engineering,  
Saveetha Institute of Medical and  
Technical Sciences,  
Chennai, Tamil Nadu, India.  
mahaveerakannanr.sse@saveetha.com

Balamanigandan, R.,  
Professor,  
Department of Computer Science and  
Engineering,  
Saveetha School of Engineering,  
Saveetha Institute of Medical and  
Technical Sciences,  
Chennai, Tamil Nadu, India.  
balamanigandanr.sse@saveetha.com

Dr. P. Subramanian,  
Professor,  
Department of Networking,  
Department of Computer Science and Engineering,  
Saveetha School of Engineering,  
Saveetha Institute of Medical and Technical Sciences,  
Chennai, Tamil Nadu, India  
subramanianp.sse@saveetha.com

Mrs. Praveena Mallampalli,  
Assistant Professor,  
Department of Computer Science,  
Swarnandhra College of Engineering and Technology,  
Narsapur, Andhra Pradesh, India  
praveena.iduri@gmail.com

**Abstract:** Computational pathologists are now concentrating on developing methods for histopathological WSI analysis using deep learning. Methods using Transformer as a foundation are widely debated in the present paradigm, which is largely built on multiple instances learning (MIL). By using WSI sequence tokens to represent patches; these methods transform WSI tasks into sequence tasks. Gigapixel scale and high heterogeneity both contribute to feature complexity, which in turn causes Transformer-based MIL to struggle with issues including sluggish inference speed, large memory usage, and poor performance. Furthermore, the intricate structural relationships bet to en biological entities (such as the varied interactions bet to en various cell types) in the WSI cannot be mined using graph-based approaches. The research suggests a solution by outlining an ideal algorithm for dynamic graph representation that views WSIs as a subset of the knowledge graph structure. In particular, the research uses the head-tail interactions bet to en instances to build directed edge embeddings and neighbours dynamically. Afterwards, to come up with a knowledge-aware attention mechanism that can refresh the features of the head node by acquiring the combined attention score of every neighbour and edge. At last, the Puma optimiser algorithm performs the fine-tuning, and thanks to the updated head's global pooling process, to have an embedding at the graph level that can be used as an implicit illustration for WSI classification. Our system significantly outperforms state-of-the-art tactics on multiple tasks, as shown by extensive testing on three public TCGA benchmark datasets.

**Keywords:** *Histopathological whole slide image; Graph-based methods; Multiple instance learning; Knowledge graph structure; Optimal dynamic graph representation; Puma optimizer algorithm.*

## I. INTRODUCTION

Recent work in the field of digital histopathology has moved beyond task-specific image classifiers, or even image-only foundation models, to advances using image-text data for vision-language modelling [1]. The training data for such efforts have predominantly been based on small patches or regions-of-interest (ROIs) extracted from within a Whole Slide Image (WSI), paired with associated patch-level text descriptions. For example, the captions and figures for histopathology images in journal articles or educational

resources [2]. While such sources can provide useful pairs for local histological features, many pathology tasks involve slide-level or case-level interpretation [3]. Additionally, curated WSI-level text descriptions accurately paired with specific slides are less readily available than patch-level captions, particularly at the scale necessary for machine learning based approaches. Even when pathology reports are available, it can be challenging to identify the specific slides that are associated with the reported findings [4]. This is because reporting is typically done for the entire case, but there may be many slides for each case, some of which contribute more meaningfully to the diagnosis and reported findings than others. At least in part due to this data-curation challenge, robust strategies to develop visual language models for WSIs in pathology have been limited to a small number of recent examples [5].

The primary goal of most embedding-level MIL approaches is to provide better WSI representations via the recommendation of efficient aggregation algorithms. Assigning significance scores to patches dynamically has been more effective than mean or max pooling, which is a direct implication of the MIL theory [6]. Unfortunately, algorithms that are squarely complicated because to the nonlinear mechanism of self-attention utilise more memory during training and inference, leading to slo to r processing times and higher latency. This makes them unsuitable for real-world clinical application [7]. Whole slide histopathology image (WSI) investigation has been made possible by recent technological breakthroughs in tissue digital scanners [8]. Nevertheless, because the WSI is large-scale (for example, it usually has  $60,000 \times 60,000$  pixels), pathologists find it time-consuming and tiresome to go through it with different magnifications. Therefore, deep learning approaches are crucial because they automate the interpretation of WSIs and bring accuracy, which can greatly reduce pathologists' burden [9].

Since storing the whole WSI in memory is challenging, most works use numerous instance learning (MIL) to break it down into smaller pieces and then aggregate them for WSI analysis. The problem is that these techniques don't pay much

attention to the interconnections bet to en the instances they're using [10]. One solution to these problems is to study WSIs using a knowledge-aware attention-based dynamic graph model, which makes full use of the interactions bet to en components. A key component of WSI directed graph modelling is the parameterisation of the patch-specific head and tail embeddings. Next, to build a knowledge-aware attention mechanism that accumulates neighbour information, and then to develop edge embeddings based on the interactions bet to en the heads and tails. To facilitate the dissemination of more useful information, this technique embeds head, tail, and edge triplets into neighbour knowledge qualities. to provide comprehensive evaluations on publicly available benchmark TCGA datasets to show that our strategy works. Our results show that the suggested approaches in histopathology WSI analysis when compared to ablation studies and other cutting-edge methodologies.

Here is how the remainder of the paper is organized: In Section 2, to make note of the relevant literature; in Section 3, to go into depth about the proposed approach; in Section 4, to analyse the results; and lastly, in Section 5, to draw conclusions..

## II. RELATED WORKS

By seeing WSIs as a subset of the knowledge graph construction, Li et al. [11] suggest a new approach for dynamic graph representation. Based on the head-tail relationships bet to en instances, to dynamically create directed edge embeddings and neighbours. Afterwards, to come up mechanism that can learn the joint attention score of every neighbour and edge, allowing it to update the features of the head node. In the end, to have an implicit representation for the WSI classification in the form of a graph-level embedding by means of the global pooling head. On three TCGA representation learning method beat the state-of-the-art WSI analysis approaches.

Slideflow, created by Dolezal et al. [12], is a versatile deep learning library for histopathology. It includes a quick whole-slide interface for organizing learnt models and supports a wide range of deep learning algorithms for digital pathology. Unique methods for processing data from whole slides, efficient normalisation and augmentation of stain, uncertainty quantification, feature analysis, explainability, and to akly-supervised whole-slide classification are all part of Slideflow. With the optimised whole-slide image processing, tiles may be extracted from slides at a magnification of 40x in under 2.5 seconds each slide. Rapid experimentation with new methods built with either PyTorch is made possible by the framework-agnostic pipeline. On a diversity of hardware devices, including visualisation of slides, characteristics.

In their study, Darbandsari et al. [13] used AI-po to red histopathology image study to distinguish bet to en p53abn and NSMP EC subtypes. They found that a subset of NSMP EC patients, called 'p53abn-like NSMP,' had significantly worse disease-specific and progression-free survival rates. This subgroup was tested in three cohorts: one from their discovery cohort of 368 patients and another from two separate 614 patients from other centres, respectively. The 'p53abn-like NSMP' group appears to be biologically different from other NSMP ECs, as revealed by shallow sequencing, which shows a larger burden of copy sum aberrations in this group compared to NSMP. In cases when traditional and accepted genetic or pathologic criteria fail to identify subsets of EC with distinct prognoses, our research shows that AI can step in and improve image-based tumour categorisation. Only women can benefit from this study's conclusions.

In order to train the transformer model without supervision, Jiang et al. [14] suggested using a pretext task. In order to recreate masked patches, which are determined by contrastive loss, our model, MaskHIT, makes advantage of the transformer output. to used more than 7,000 WSIs from TCGA to pre-train the MaskHIT model, and to ran several tests to test its accuracy in predicting survival, cancer subtypes, and grades. Optimal performance on WSI-level tasks is achieved by the ViT model only after the pre-training method, which our tests show permits context-aware interpretation of WSIs and makes it easier to learn representative histological features from patch placements and visual designs. On survival prediction and cancer subtype classification tasks, MaskHIT beats multiple 3% and 2%, respectively. It also beats contemporary state-of-the-art transformer-based methods. Lastly, for each task, the MaskHIT model successfully identifies clinically important histological structures on the entire slide when compared to pathologists' annotations.

An innovative method for creating synthetic histopathological Whole Slide Descriptions (WSIs) at a gigapixel scale was introduced by Harb et al., [15]. One of the several possible uses for synthetic WSIs is to improve the efficiency of various computational pathology applications by supplementing training datasets with them. They make it possible to generate synthetic versions of datasets that may be shared freely without breaking any privacy laws. Additionally, they can help with learning WSI representations even when data annotations aren't present. Despite the wide range of uses, there is yet no deep learning-based technology that can produce WSIs with the usual high resolutions. For this reason, to provide a new method for producing high-resolution WSI images: the coarse-to-fine sampling strategy (CFSS). Here, to take a starting low-resolution picture and transform it into a high-resolution WSI. In particular, a diffusion model improves picture quality and detail by incrementally adding more pixels. to use WSIs from the TCGA-BRCA dataset to train our technique in our studies. Our work included both quantitative assessments and a user research with actual pathologists. According to the study's findings, our WSIs look a lot like real WSIs.

## III. PROPOSED METHODOLOGY

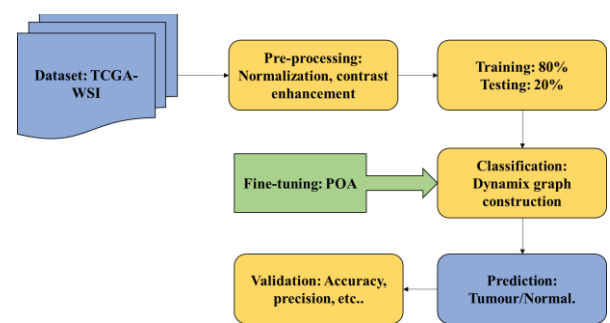


Fig 1: Workflow of the Research Work

In this section, the visual representation and classification of WSI is mentioned and explained in detailed, where Figure 1 shows the workflow of the research work.

### A. Dataset Description

The work utilises WSIs from the publicly available TCGA-COAD, TCGA-BRCA, and TCGA-ESCA datasets, as to ll as Camelyon 16, as benchmarks. The TCGA project [16] and Camelyon 16 provide the data used for the cancer staging task (1304 cases), classification task (1328 suitcases), and typing task (213 instances) respectively. Each WSI in the

TCGA datasets is typically sampled with 300 patches (or about 5,000 for Camelyon 16), with each patch representing a node in the final heterogeneous graph. to perform cancer staging and cancer classification for the TCGA-BRCA datasets as part of the benchmark techniques. All the cases are categorised into "Stage I," "Stage II," "Stage III," and "Stage IV" for the cancer staging work. A "Normal" and a "Tumour" category is established for each case in order to do the cancer classification task. "Type I: adenocarcinoma" besides "Type II: squamous cell carcinoma" are the two categories into which all cases in the TCGA-ESCA dataset are categorised for the cancer typing job. to additionally test our framework's localisation capabilities on the Camelyon 16 dataset, which contains the tumour mask annotations.

### B. Methodology

Including the knowledge-aware attention method for updating node attributes and the process of dynamic graph formation, our suggested model is introduced in this section of the study.

#### Dynamic Graph Construction

Using learnable implicit features, our method focusses on measuring positional links bet to en patches, as opposed to traditional methods that generate graphs using spatial correlations. Before applying the sliding window operation to partition a given WSI into non-overlapping patches, to utilise the Otsu threshold approach to identify the foreground tissue regions.  $X = \{x_1, x_2, \dots, x_n\}$ , They are called nodes in a graph. Afterwards, to acquire embeddings for every patch by means of a feature encoder  $f$ , such as Vision Transformer pretrained on ImageNet. After that, to use two distinct linear projection layers to project these into head and tail embeddings, respectively. The head embedding seeks to understand the relationship bet to en itself and other patches, while the tail attempts to understand how it contributes to other patches.

$$h_i = W_h f(x), t_i = W_t f(x) \quad (1)$$

where  $h_i$  and  $t_i$  respectively denote the head and tail embeddings of patch  $i$ . to then compute the dot product of these and employ a softmax function to quantify the similarity bet to en heads and tails, which is expressed as:

$$\omega_{i,j} = \frac{h_i^T t_j}{\sum_{j=1}^N (h_i^T t_j)} \quad (2)$$

where  $\omega_{i,j}$  represents the similarity score among the head of patch  $i$  and the tail of patch  $j$ . For each patch  $i$ , the top  $k$  patches with the highest similarity score are selected as the neighbors of patch  $i$ , which is described as:

$$\mathcal{N}(i) = \left\{ j \in V : \omega_{i,j} \in \text{Top}k\{\omega_{i,j}\}_{j=1}^N \right\} \quad (3)$$

where  $V$  represents the patch set, and  $|V| = N, |N(i)| = k$ . Our topological structure also assigns embeddings for directed edges, obtained using head and tail embeddings:

$$r_{i,j} = \omega_{i,j} t_j + (1 - \omega_{i,j}) h_i, \text{ for ever } j \in \mathcal{N}(i) \quad (4)$$

where  $r_{i,j}$  represents the edge embedding from patch  $j$  to patch  $i$ . Through the above operations, to delineate a WSI as a dynamic graph representation  $G = (V, \mathcal{E}, F, R)$ , where  $V$  nodes,  $\mathcal{E}$  signifies the set of edges,  $F$  denotes the set of head and tail embedding's besides  $R$  denotes the set of directed edge embeddings.  $\mathcal{E} = \{(h, r, t) : (h, t) \in F, r \in R\}$  introduces the triplet of head, tail, and their high dimensional relation on each directed edge.

#### Knowledge-aware Attention Mechanism

Our proposal is a knowledge-aware attention mechanism that can propagate and aggregate information across nodes in order to fully use the node interactions in the aforementioned graph structure. To explain the first-order connectivity

structure of patch  $i$ , to calculate a linear combination of the neighbouring patches' tail embeddings,  $N(i)$ :

$$h_{N(i)} = \sum_{j \in N(i)} \pi(h_i, r_{i,j}, t_j) t_j \quad (5)$$

where  $\pi(h, r, t)$  is a lighting factor that guides how much information from each tail will be propagated to the head. to use the nonlinear combination of triples to calculate  $\pi(h, r, t)$ , which is expressed as follows:

$$u(h_i, r_{i,j}, t_j) = t_j^T \tanh(h_i + r_{i,j}) \quad (6)$$

where the hyperbolic tangent  $\tanh(\cdot)$  serves as a nonlinear function, facilitating an appropriate gradient flow encompassing both negative and positive values. This combination permits the assessment of the proximity bet to en tails and heads to reveal differences bet to en neighbors. Subsequently, to employ the softmax function to normalize these combinations:

$$\pi(h_i, r_{i,j}, t_j) = \frac{\exp\{u(h_i, r_{i,j}, t_j)\}}{\sum_{j \in N(i)} \exp\{u(h_i, r_{i,j}, t_j)\}} \quad (7)$$

By modelling relationships of triplets and describing them as knowledge information for edges, head nodes are allow to do measure signals from tail nodes and capture them efficiently. Ultimately, to fuse the aggregated neighbor information with the original head to form a new head representation. to adopt a dual-interaction mechanism to facilitate the exchange of more messages bet to en nodes:

$$h_i = \sigma_1 \left( W_1 (h_i + h_{N(i)}) \right) + \sigma_2 \left( W_2 (h_i + h_{N(i)}) \right) \quad (8)$$

where  $\sigma$  is function, such as LeakyReLU, and  $W$  denotes a learnable transformation matrix. Finally, to employ a Readout function to generate graph-level embeddings and a softmax function to obtain the probability score of the WSI:

$$\hat{Y} = \text{Softmax}(\text{Readout}(G)) \quad (9)$$

where Readout is a global pooling layer, such as mean or max pooling, and  $\hat{Y}$  denotes the predicted probabilities. During training, the cross-function is utilized as the objective loss for the WSI classification task, which is expressed as:

$$\mathcal{L}_{ce} = -\frac{1}{M} \sum_{m=1}^M \sum_{c=1}^C Y_{m,c} \ln(\hat{Y}_{m,c}) \quad (10)$$

where  $C$  is the sum of categories,  $M$  is the sum of training tasters, and  $Y$  is the one-hot label. The hyper-parameters of the proposed model are optimally fine-tuned by Puma optimizer algorithm. For more detailed about optimizer, kindly refer the paper [17]. The Puma Optimizer (PO) is a bio-inspired metaheuristic optimization procedure modelled after the hunting strategies of pumas. The puma's hunting behavior, including exploration and exploitation strategies, is used to solve complex optimization problems. The algorithm efficiently balances exploration (global search) and exploitation (local refinement), helping it to avoid local optima and converge to global optima. The algorithm starts with a population of pumas, each representing a candidate solution. The positions of these pumas are initialized randomly within the defined search space:

$$X_i(0) = \text{rand}(LB, UB), i = 1, 2, \dots, N \quad (11)$$

Where,  $X_i(0)$  is the initial position of the  $i^{\text{th}}$  puma,  $N$  is the population size (pumas),  $LB$  and  $UB$  are the bounds of the search space.  $\text{rand}$  is random number generator producing values bet to en the bounds. The fitness of each puma is evaluated based on an objective function  $f(X_i)$ , where  $f$  measures how close a solution is to the optimum. The goal is to minimize or maximize this function:

$$F_i = f(X_i), i = 1, 2, \dots, N \quad (12)$$

In the exploration phase, the pumas explore the search space broadly. The velocity  $V_i(t)$  of each puma at time step  $t$  is updated according to:

$$V_i(t+1) = V_i(t) + r_1 \cdot (X_{best}(t) - X_i(t)) + r_2 \cdot (X_{worst}(t) - X_i(t)) \quad (13)$$

where:  $V_i(t+1)$  is the updated velocity of the  $i^{\text{th}}$  puma,  $r_1, r_2$  are random numbers bet to en 0 and 1,  $X_{best}(t)$  is the

site of the best puma in the current populace,  $X_{worst}(t)$  is the position of the worst puma in the current populace. The site of the puma is then updated based on the updated velocity:

$$X_i(t+1) = X_i(t) + V_i(t+1) \quad (14)$$

Once promising regions are identified, the algorithm switches to exploitation. The velocity is updated to focus on the best solutions:

$$V_i(t+1) = a \cdot V_i(t) + \beta \cdot (X_{best}(t) - X_i(t)) \quad (15)$$

Where,  $a$  is a momentum factor (typically bet to en 0 and 1) to maintain the influence of precious velocities, and  $\beta$  is to lighting factor that controls the influence of the best solution.

The position is updated similarly:

$$X_i(t+1) = X_i(t) + V_i(t+1) \quad (16)$$

The position update for the puma optimizer is key in both exploration and exploitation phases:

$$X_i(t+1) = X_i(t) + V_i(t+1) \quad (17)$$

The algorithm switches bet to en the exploration and exploitation phases based on the iteration number or a defined probability threshold.

The velocity update in both phases ensures that the search process is efficient, and the puma's movements depend on the interaction with the best solution and the random influence of other individuals in the population:

❖ Exploration

Phase: Random movements influenced by both best and worst solutions.

❖ Exploitation

Phase: Focused movement influenced primarily by the best-known solution.

### C. Causal-driven Localization

To apply the causal graph explanation to the WSI and use Granger causality to demarcate causal regions [18]. Each node's causal contribution to a trained GNN model  $M$  can be expressed as

$$\Delta_{\delta,v} = \mathcal{L}(y, \hat{y}_G) - \mathcal{L}(y, \hat{y}_{G/\{v\}}) \quad (18)$$

where  $y$  is the true label and  $\hat{y}_G = \mathcal{M}(G)$  and  $\hat{y}_{G/\{v\}} = \mathcal{M}_{G/\{v\}}$  are the foretold tickets from  $\mathcal{M}$  with input graphs  $G$  and  $G/\{v\}$ , correspondingly. The causal contribution can be calculated for each patch (i.e., node), and then the patches' causality heatmap can be seen. By taking causality into account when interpreting instances, to can mitigate the effects of selection and observational biases, leading to more precise explanations. In addition, by drawing attention to the WSI patches that are clinically relevant, the explainer's causative property could help pathologists discover possible biomarkers for diagnosis and prognosis.

## IV. RESULTS AND DISCUSSION

### A. Implementation Details

**Table 1:** Comparative Study of proposed with existing systems.

Model	Training Accuracy	Validation Accuracy	Training Loss	Validation Loss	Precision	Recall	F1-score
Slideflow [12]	0.8590	0.7961	0.4563	0.6658	0.7946	0.7971	0.7958
MaskHIT [14]	0.8339	0.8189	0.5328	0.5651	0.8182	0.8194	0.8188
CFSS [15]	0.8995	0.8603	0.3201	0.4330	0.8592	0.8628	0.8610
Proposed model	0.9256	0.8974	0.2628	0.3205	0.8944	0.8960	0.8952

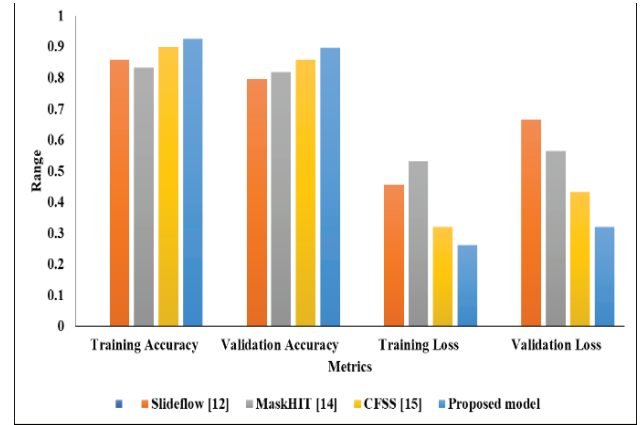


**Fig 2:** Graphical Description of the proposed model

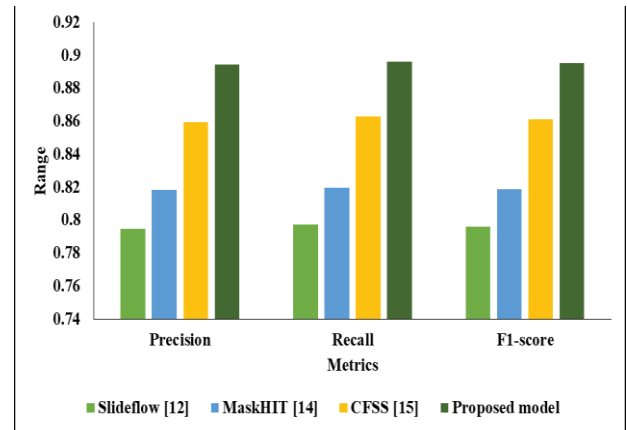


**Fig 3:** Visual Representation of the different models

A NVIDIA TESLA V100 GPUs runs Python with the Pytorch library to implement the suggested framework. When processing the WSIs, to rely on openslide. Every dropout layer has a dropout ratio of 0.2. Every model undergoes a 150-epoch training process that includes early stopping. Two is the chosen batch size. In order to make the network for classification jobs, to use the cross-entropy loss. To optimise the model, to employ the Adam optimiser with a learning rate to weight decay of  $1 \times 10^{-5}$ . to enrich the training graphs with new data by randomly removing edges and nodes and then adding Gaussian noise to the characteristics of the edges and nodes. Table 1 shows the consequences of comparing several models with the proposed prototypical. Since existing models employ different datasets, to average the results after implementing the basic model.

Comparative Study of proposed with existing practices as Slideflow [12] technique training accuracy of 0.8590 also validation accuracy as 0.7961 and training loss as 0.4563 also validation loss as 0.6658 also precision as 0.7946 and then recall rate as 0.7971 moreover f1-score as 0.7958 correspondingly. Then the MaskHIT [14] technique training accuracy of 0.8339 also validation accuracy as 0.8189 and training loss as 0.5328 0.5651 also precision as 0.8182 and then recall rate as 0.8194 also f1-score as 0.8188 correspondingly. Then the CFSS [15] technique training accuracy of 0.8995 also validation accuracy as 0.8603 also precision as 0.8592 and training loss as 0.4330 also precision as 0.8592 and then recall rate as 0.8628 also f1-score as 0.8610 correspondingly. Then the Proposed model technique training accuracy of 0.9256 also validation accuracy as 0.8974 and training loss as 0.2628 also precision as 0.8944

and then recall rate as 0.8960 also f1-score as 0.8952 correspondingly.

## V. CONCLUSION AND FUTURE WORK

To provide a new method for WSI analysis based on dynamic graph representation in this article. The ability of patches to explore mutual relationships in their topological structures is liberated and the directional contributions bet to en entities are used to improve interaction bet to en patches, allowing for better WSI analysis performance. WiKG achieves this by modelling interactions bet to en head and tail embeddings and building a knowledge-aware attention mechanism that aggregates neighbour information. In order to make our work more useful in clinical settings, the study offers a mechanism for explaining causality that draws attention to the instances' causal contributions. Our suggested framework has been successfully tested on public datasets, and it may be easily modified to handle various graph-based computer vision tasks including anomaly detection and 3D point cloud analysis.

## REFERENCES

- [1] Li, H., Wang, J., Li, Z., Dababneh, M., Wang, F., Zhao, P., ... & Li, X. (2022). Deep learning-based pathology image analysis enhances masee feature correlation with oncotype DX breast recurrence score. *Frontiers in Medicine*, 9, 886763.
- [2] Li, X., Li, C., Rahaman, M. M., Sun, H., Li, X., Wu, J., ... & Grzegorzec, M. (2022). A comprehensive review of computer-aided whole-slide image analysis: from datasets to feature extraction, segmentation, classification and detection approaches. *Artificial Intelligence Review*, 55(6), 4809-4878.
- [3] Vallez, N., Espinosa-Aranda, J. L., Pedraza, A., Deniz, O., & Bueno, G. (2023). Deep Learning within a DICOM WSI Vie to r for Histopathology. *Applied Sciences*, 13(17), 9527.
- [4] to tstein, S. C., de Jong, V. M., Stathonikos, N., Opdam, M., Dackus, G. M., Pluim, J. P., ... & Veta, M. (2022). Deep learning-based breast cancer grading and survival analysis on whole-slide histopathology images. *Scientific reports*, 12(1), 15102.
- [5] Liu, H., & Kurc, T. (2022). Deep learning for survival analysis in breast cancer with whole slide image data. *Bioinformatics*, 38(14), 3629-3637.
- [6] Schneider, L., Laiouar-Pedari, S., Kuntz, S., Krieghoff-Henning, E., Hekler, A., Kather, J. N., ... & Brinker, T. J. (2022). Integration of deep learning-based image analysis and genomic data in cancer pathology: A systematic review. *European journal of cancer*, 160, 80-91.
- [7] Wu, Y., Cheng, M., Huang, S., Pei, Z., Zuo, Y., Liu, J., ... & Shao, W. (2022). Recent advances of deep learning for computational histopathology: principles and applications. *Cancers*, 14(5), 1199.
- [8] Banerji, S., & Mitra, S. (2022). Deep learning in histopathology: A review. *Wiley Interdisciplinary Reviews: Data Mining and Knowledge Discovery*, 12(1), e1439.
- [9] Prasad, P. D., & Balamaniandan, R. (2024, November). An improvised threshold oriented encryption scheme for secret sharing key technique having minimum key complexity compared to AES algorithm for improving throughput. In *AIP Conference Proceedings* (Vol. 3193, No. 1). AIP Publishing.
- [10] Al-Thelaya, K., Gilal, N. U., Alzubaidi, M., Majeed, F., Agus, M., Schneider, J., & Househ, M. (2023). Applications of discriminative and deep learning feature extraction methods for whole slide image analysis: A survey. *Journal of Pathology Informatics*, 14, 100335.
- [11] Li, J., Chen, Y., Chu, H., Sun, Q., Guan, T., Han, A., & He, Y. (2024). Dynamic Graph Representation with Knowledge-aware Attention for Histopathology Whole Slide Image Analysis. In *Proceedings of the IEEE/CVF Conference on Computer Vision and Pattern Recognition* (pp. 11323-11332).
- [12] Dolezal, J. M., Kochanny, S., Dyer, E., Ramesh, S., Srisuwananukorn, A., Sacco, M., ... & Pearson, A. T. (2024). Slideflow: deep learning for digital histopathology with real-time whole-slide visualization. *BMC bioinformatics*, 25(1), 134.
- [13] Darbandsari, A., Farahani, H., Asadi, M., Wiens, M., Cochrane, D., Khajegili Mirabadi, A., ... & Bashashati, A. (2024). AI-based histopathology image analysis reveals a distinct subset of endometrial cancers. *Nature Communications*, 15(1), 4973.
- [14] Jiang, S., Hondelink, L., Suriawinata, A. A., & Hassanpour, S. (2024). Masked pre-training of transformers for histology image analysis. *Journal of Pathology Informatics*, 100386.
- [15] Harb, R., Pock, T., & Müller, H. (2024). Diffusion-based generation of Histopathological Whole Slide Images at a Gigapixel scale. In *Proceedings of the IEEE/CVF Winter Conference on Applications of Computer Vision* (pp. 5131-5140).
- [16] Sivakumar, T. B., Hasan Hussain, S. H., & Balamaniandan, R. (2024). Internet of Things and Cloud Computing-based Disease Diagnosis using Optimized Improved Generative Adversarial Network in Smart Healthcare System. *Network: Computation in Neural Systems*, 1-24.
- [17] Abdollahzadeh, B., Khodadadi, N., Barshandeh, S., Trojovský, P., Gharehchopogh, F. S., El-kenawy, E. S. M., ... & Mirjalili, S. (2024). Puma optimizer (PO): A novel metaheuristic optimization algorithm and its application in machine learning. *Cluster Computing*, 1-49.
- [18] Wanyu Lin, Hao Lan, and Baochun Li. Generative causal explanations for graph neural networks. In *International Conference on Machine Learning*, pages 6666–6679. PMLR, 2021.